J Adv Ceram

Research Article

Exceptional thermal shock resistance of RSZ/YSZ coatings for rocket engines at 1800 °C

Lin Chen[1], Yu-Xing Guo[1], Chao Li[2], Hong-Xu Zhang[2], Cheng-Bin Zheng[2], Guo-Qiang Wang[2], Chang-Jiu Li[1], Guan-Jun Yang[1,✉]

Cite this article: Chen L, Guo Y-X, Li C, et al. *J Adv Ceram* 2026, **15**(2): 9221228. https://doi.org/10.26599/JAC.2025.9221228

ABSTRACT: To meet the demands for high thrust-to-weight ratios and reusability, rocket engines require thermal barrier coatings (TBCs) capable of withstand 1800 °C for prolonged durations. This study presents a novel quaternary rare earth-stabilized cubic zirconia (RSZ) material and systematically optimizes double-ceramic-layer (DCL) RSZ/yttria-stabilized zirconia (YSZ) coating architectures. The optimized structure—with a total thickness of 350 μm and a YSZ-to-RSZ thickness ratio of 1 : 1—exhibits outstanding thermal shock resistance at 1800 °C, achieving a lifespan of 15 cycles and thereby satisfying the performance benchmark for rocket engines under such extreme conditions. In this optimized configuration, failure proceeds through sintering-induced localized spallation, a comparatively gradual process that contributes to prolonged coating durability. These findings highlight the strong potential of RSZ/YSZ coatings for application in next-generation rocket engines operating at 1800 °C.

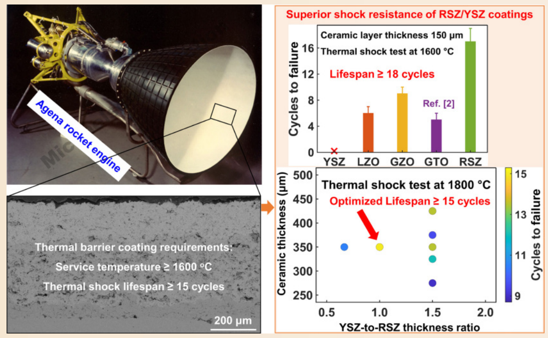

KEYWORDS: thermal barrier coatings (TBCs); rocket engines; thermal shock; spallation; lifespan

1 Introduction

To meet the growing demands for high thrust-to-weight ratios and reusability, modern rocket engines extensively utilize lightweight, thin-walled structural designs. These components, such as rocket thrust chambers and first-stage boosters (sea level), are constructed from nickel superalloys and are characterized by their minimal thickness (less than 1.0 mm), complex geometries, and stringent weight constraints [1]. However, during operation, they are subjected to gradient thermal shock from gases at temperatures reaching 3000 K and pressures exceeding 5 MPa [2]. Although regenerative cooling technology is employed for these components [3,4], the surface temperature remains close to the melting point of nickel superalloys (1250–1400 °C), significantly shortening their operational lifespan.

The application of thermal barrier coatings (TBCs) has become crucial for protecting metallic substrates from high-temperature oxidation and corrosion while lowering substrate temperatures. Compared with the TBCs used in aerospace or gas turbine engines [5], coatings in rocket engines face significantly higher operating temperatures, often exceeding 1600 °C. Moreover, to achieve a sufficiently high thrust-to-weight ratio, a surface temperature of 1600 °C is considered a baseline, with an ultimate target of 1900 °C.

Owing to its balanced properties—low thermal conductivity, high fracture toughness, and high thermal expansion coefficient—8 wt% yttria-stabilized zirconia (YSZ) remains the benchmark TBC material used in aeroengines and gas turbines [6]. However, our preliminary studies revealed that a pure YSZ coating lasts less than 90 s under thermal shock at 1600 °C and fewer than 2 cycles at 1550 °C [2]. Therefore, there is an urgent need to develop new ultrahigh-temperature TBCs suitable for rocket engine applications.

Significant research efforts have been directed toward identifying alternatives to YSZ. Double-ceramic-layer (DCL) TBCs, which are commonly used in aeroengines and gas turbines, have shown promise [5,7,8]. In such systems, a new material serves as the topcoat, whereas a YSZ intermediate layer mitigates the thermal stress between the topcoat and the substrate. Among the candidate materials, lanthanum zirconate ($La_2Zr_2O_7$ (LZO)) [9,10], gadolinium zirconate ($Gd_2Zr_2O_7$ (GZO)) [11,12], and gadolinium tantalate ($GdTaO_4$ (GTO)) [13,14] have exhibited potential. While these materials achieve lower thermal conductivity than YSZ does, they often suffer from low fracture toughness and thermal expansion coefficients, which promote crack propagation. Furthermore, their performance is typically evaluated below 1400 °C [5], which corresponds to the operational range of aeroengines and gas turbines. Importantly, coatings

[1]School of Materials Science and Engineering, Xi'an Jiaotong University, Xi'an 710049, China. [2]Xi'an Space Engine Company Limited in China Aerospace Science and Technology Co., Xi'an 710065, China.

✉ Corresponding author. E-mail: ygj@xjtu.edu.cn

Received: August 27, 2025; Revised: November 17, 2025; Accepted: December 9, 2025

demonstrating excellent durability at 1400 °C may undergo fundamental changes in failure behavior at 1600 °C or above, as encountered in rocket engines. This is supported by the significant decrease in the thermal shock lifespan of YSZ coatings at 1600 °C [2] compared with those at 1300 °C [15] and 1400 °C [16].

Thermal shock resistance is one of the most critical performance metrics for rocket engine TBCs. However, conventional gradient thermal shock tests for aeroengines and gas turbines are typically conducted with a small temperature gradient within the coatings (less than 300 K) and a low cooling rate (less than 50 $K \cdot s^{-1}$). These conditions are not representative of rocket engine environments, which require a large temperature gradient (greater than 500 K) and a high cooling rate (greater than 100 $K \cdot s^{-1}$). For example, YSZ TBCs exhibited a lifespan reduction by a factor of 2–3 when the cooling rate increased from 10 to 100 $K \cdot s^{-1}$ in a burner rig test [6]. Therefore, systematic investigations into the ultrahigh-temperature thermal shock behavior of TBCs under rocket engine–relevant conditions are essential for identifying suitable coatings for use at 1600 °C and above.

In this study, a novel quaternary rare earth-stabilized cubic zirconia (RSZ) material—composed of 10.6 mol% (Y_2O_3, Yb_2O_3, Gd_2O_3, and Nd_2O_3)-stabilized cubic ZrO_2—and corresponding RSZ/YSZ DCL TBCs were specifically developed for rocket engine applications. For comparison, several coatings commonly applied in aeroengines and gas turbines (LZO/YSZ, GZO/YSZ, and GTO/YSZ) were selected, along with a pure YSZ baseline coating. To simulate real service environments, gradient thermal shock tests were conducted at temperatures up to 1900 °C. The coating architecture was systematically optimized to extend the operational limits, and the underlying failure mechanisms were identified. The results demonstrate that the RSZ/YSZ DCL coatings, with a total ceramic thickness of 350 μm and a YSZ-to-RSZ thickness ratio of 1 : 1, exhibit superior thermal shock resistance at 1800 °C, achieving a lifespan of 15 cycles. This meets the typical performance requirements for rocket engines under such extreme conditions, demonstrating the strong potential of RSZ/YSZ DCL TBCs for application in rocket engines operating at temperatures up to 1800 °C.

2 Experimental

2.1 Coating preparation

Five types of coatings—pure YSZ, LZO/YSZ, GZO/YSZ, GTO/YSZ, and RSZ/YSZ—were prepared to assess their suitability for rocket engine applications. The TBCs were deposited on nickel superalloys (Inconel 738, ϕ25.4 mm × 3 mm) via a commercial atmospheric plasma spray (APS) system (ZB-80, Hebei Zhenbang Aerospace Precision Machinery Co., Ltd., China). The system was equipped with a gun (9MBM, Oerlikon Metco, Switzerland) and a powder feeder (ZB80F, Hebei Zhenbang Aerospace Precision Machinery Co., Ltd., China). All the ceramic layers were sprayed under identical parameters, as detailed in Table 1. The particle sizes of the bond coat (BC; MCrAlY, Amdry 365-2, Oerlikon Metco, Switzerland), YSZ (YSZ1001AS, Xi'an Aerospace Composites Research Institute, China), LZO (Jiorie Thermal Spray Materials Co., Ltd., China), and GZO (Beijing United Coating Technology Co., Ltd., China) powders were 38–75, 45–75, 45–75, and 11–53 μm, respectively. RSZ powders were synthesized via hydrothermal methods, followed by agglomeration, granulation, and sintering, achieving a final particle size of 11–53 μm. Similarly, GTO powders were prepared via a two-step sintering process and subsequent mechanical crushing [2], resulting in a particle size distribution of 45–75 μm. Prior to coating deposition, the nickel superalloy substrates were grit-blasted with 40–60 mesh Al_2O_3 grits to achieve an average roughness (R_a) of 5–10 μm. The thickness of the BC was controlled at 70±20 μm. The YSZ intermediate layer and topcoat thicknesses ranged from 90 to 255 μm and from 60 to 215 μm, respectively, resulting in a total ceramic layer thickness ranging from 150 to 425 μm.

2.2 Gradient thermal shock at 1600–1800 °C

Regenerative cooling in rocket engine thrust chambers and nozzles induces a large temperature gradient across the TBC [1,3], making thermal shock resistance a key performance metric. Thermal shock tests were performed according to the Chinese national standard GB/T 42261. A supersonic gun generated a high-temperature flame perpendicular to the sample surface at a boundary velocity of approximately 2000 $m \cdot s^{-1}$. The TBC surface was heated to 1600–1800 °C via a kerosene-oxygen flame, whereas the substrate backside was cooled to below 600 °C via water at a flow rate of 430–600 $mL \cdot min^{-1}$. Further test details are provided in our earlier work [2]. The sample surface temperature was monitored via a noncontact two-color pyrometer (E1RH-F2-L-0-0, Fluke, Germany), with a calibration slope of 1.05 for the current coating. Prior to testing, the thermal history during a single cycle was recorded, revealing temperature fluctuations within 30 °C. During testing, the samples underwent rapid heating and cooling at 100 $K \cdot s^{-1}$, with a through-thickness temperature gradient exceeding 500 K. At least two samples were tested per group.

2.3 Isothermal thermal cycling test at 1130 °C

For radiatively cooled nozzles such as the Merlin vacuum expansion nozzle [4], coatings experience near-isothermal cycling at approximately 1200 °C. Thermal cycling tests were conducted following the national standard GB/T 42259 via a muffle furnace (SX-Q08163, Tianjin Zhonghuan Electric Furnace Co., Ltd., China). The samples were placed directly into the furnace at 1130 °C, held for 10 min, then removed and quenched in cold water. The coating lifespan was defined as the number of cycles until 5% of the coating area spalled. The spalled area was quantified via ImageJ 1.45 software. At least two samples were tested per group.

2.4 Characterization of microstructures and properties

The coating surface and cross-sections were examined by a scanning electron microscope (SEM; VEGA II-XMU, TESCAN, Czech Republic). The elemental distribution was analyzed via an energy dispersive spectroscope (EDS; AZTEC, Oxford Instruments, UK) at 15 kV and a 15 mm working distance. Phase identification was carried out via an X-ray diffractometer (XRD; D8 Advance 3.0, Bruker, Germany) over a 2θ range of 10°–90°, with a step size of 0.1° and a scan speed of 2°$\cdot min^{-1}$. The thermally grown oxide (TGO) thickness was measured via Demo VegaTC software integrated with SEM. Statistical values were derived from 200 measurements per group. The coating porosity was

Table 1 APS parameters used in this study

Parameter	BC	Ceramic layer
Plasma arc power (kW)	36	42
Plasma gas (Ar, $L \cdot min^{-1}$)	45	45
Auxiliary gas (N_2, $L \cdot min^{-1}$)	7.0	7.0
Spray distance (mm)	110	90
Powder feed rate ($g \cdot min^{-1}$)	25	15

determined by binarizing SEM backscattered electron (BSE) images via ImageJ 1.45, with at least 10 images analyzed per condition.

The bond strength was tested according to the ASTM C-633 standard via a universal testing machine (Instron 1195, INSTRON Co., Ltd., USA) at a constant speed of 1.0 mm·min^{-1}. The coated samples were bonded to their counterparts via AB glue (1 : 1 mass ratio) and cured at 100 °C for 3 h. Three samples were tested per group. The cross-sectional hardness was measured with a micro-Vickers indenter (BUEHLER MICROMET 5104, Akashi Co., Japan) under a 300 g load and 30 s dwell time, following ASTM E384.

Infrared reflectance spectra of the free-standing coatings were acquired via an ultraviolet–visible–near infrared (UV-Vis-NIR) spectrophotometer (UV-3600, Shimadzu, Japan) at room temperature, covering a wavelength range of 1000–2200 nm. According to Wien's displacement law [17], blackbody emission peaks at 1600 and 1800 °C occur at 1.547 and 1.398 μm, respectively. Measurements were taken at an incidence angle of 45° and calibrated via a titanium oxide standard plate. The reflectance was recorded with an infrared integrating sphere accessory. Each wavelength was measured three times and averaged.

2.5 Finite element analysis (FEA) for coating spallation

Spallation behavior was simulated via FEA in COMSOL Multiphysics (v6.0). A 2D symmetric plane strain model was constructed with a total length four times its height. The left boundary was set as symmetric, and the bottom boundary was fixed in the *y*-direction to prevent rigid body motion. A swept mapped mesh with a minimum element size of 5 μm was used. A mesh convergence study confirmed a computational error of less than 10%. The relative tolerance was set to 0.001, yielding a final mesh of approximately 90,000 elements with an average quality of 1.0. The initial crack length was set to four times the ceramic layer thickness and propagated in 10 μm increments.

3 Results

3.1 As-sprayed coating microstructure

Figure 1 shows the cross-sectional microstructures of the as-sprayed DCL TBCs. All five types of coatings exhibit typical lamellar structures, with surface R_a values between 7 and 10 μm and bond strengths exceeding 20 MPa at a ceramic thickness of 150 μm. The measured porosities were 7.9%±1.4% for pure YSZ [2], 8.9%±1.2% for LZO/YSZ, 9.0%±1.3% for GZO/YSZ, 6.9%±1.8% for GTO/YSZ, and 7.7%±2.1% for RSZ/YSZ. No penetrating cracks or interfacial spallation were observed in any of the as-sprayed coatings.

3.2 Thermal cycling lifetime at 1130 °C

Figure 2 compares the thermal cycling lifetimes of the five types of coatings at 1130 °C. The LZO/YSZ coating fails to meet the minimum lifespan requirements of 30 cycles for typical rocket engines, which can be attributed to its low fracture toughness and thermal expansion coefficient (Table 2). This observation is consistent with previous reports: $La_2(Zr_{0.75}Ce_{0.25})_2O_7$ (Ce-LZO), Ce-LZO/YSZ, and Ce-LZO/CYSZ coatings with ceramic thicknesses of 300 μm survived only 2, 14, and 10 cycles at 1050 °C, respectively [18], and Ce-LZO has properties similar to those of LZO. Similarly, 150 μm Yb-LZO [19], 200 μm $La_2Ce_2O_7$ (LCO) [20,21], and 275 μm LZO [22] coatings endured only 15, 22, and 28 cycles at 1050, 1000, and 1100 °C, respectively. In contrast, the pure RSZ and RSZ/YSZ coatings exhibited lifespans of 50 and 105 cycles at 1130 °C, respectively, outperforming the LZO/YSZ, GZO/YSZ, and GTO/YSZ systems owing to their more favorable fracture toughness and thermal expansion coefficient (Table 2). The pure YSZ coating (150 μm) has a lifespan of 56 cycles [2], and even at 750 μm thickness, it maintained 28 cycles [23,24], confirming its high toughness. These results demonstrate the outstanding thermal cycling resistance of RSZ/YSZ coatings at 1130 °C.

Figure 3 shows the coating microstructures after thermal cycling at 1130 °C. The pure YSZ coatings failed by overall ceramic layer spallation (Fig. 3(a)), as commonly observed in thick YSZ coatings [24]. In contrast, the LZO/YSZ, GZO/YSZ, and GTO/YSZ coatings exhibited premature topcoat spallation (Figs. 3(b)–3(d)), resulting from their low fracture toughness and thermal expansion coefficient (Table 2), which is also reported for the Ce-LZO [18] and Yb-LZO [19] coatings at 1050 °C. The RSZ/YSZ coating showed both localized RSZ topcoat spallation and full ceramic layer spallation (Figs. 3(e) and 3(f)), accompanied by high densities of vertical cracks.

The average thickness of the TGO reaches 8.2 μm in the failed pure YSZ coating [2], exceeding the critical threshold of 5–6 μm [25]. This is consistent with its high oxygen diffusion coefficient [26]. In contrast, the average TGO thicknesses in the LZO/YSZ,

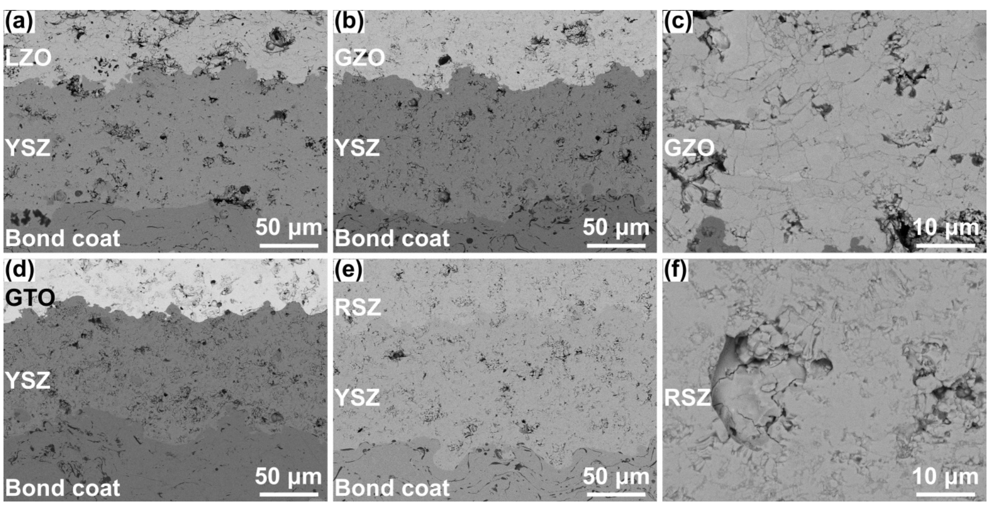

Fig. 1 Cross-sectional microstructures of DCL TBCs: (a) LZO/YSZ, (b, c) GZO/YSZ, (d) GTO/YSZ, and (e, f) RSZ/YSZ.

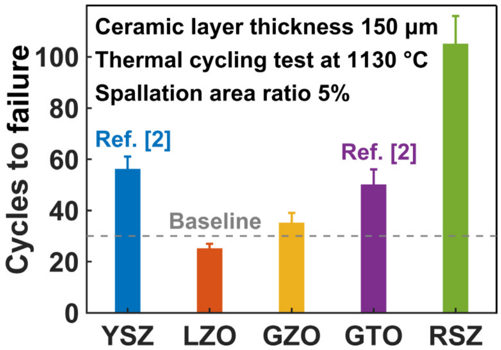

Fig. 2 Thermal cycling lifetime of DCL TBCs at 1130 °C with a ceramic layer thickness of 150 μm. Baseline indicates minimum lifespan requirement for typical rocket engines.

Table 2 Thermophysical properties of ceramic candidates for DCL TBCs

Candidate	K_{IC} (MPa·m$^{1/2}$)	κ (W·m^{-1}·K^{-1})	α (10^{-6} K^{-1})
YSZ	2.2 [27]	0.90 [28]	10.7 [29]
LZO	1.1 [30]	0.74 [15]	9.1 [9,29–31]
GZO	1.1 [27,32]	0.85 [33]	10.4 [34]
GTO	1.7 [2]	0.64 [2]	8.5 [35]
RSZ	1.5	0.60	10.1

Note: K_{IC}, κ, and α represent fracture toughness, thermal conductivity, and coefficient of thermal expansion, respectively.

GZO/YSZ, and GTO/YSZ coatings are approximately 1.5, 2.2, and 4.3 μm, respectively. These values align with the reported ranges of 1.08–2.2 μm for thermally cycled Ce-LZO/8YSZ [18] and Yb-LZO/YSZ [19] coatings at 1050 °C. Although the RSZ/YSZ coating exhibited a TGO thickness similar to that of pure YSZ, it displayed numerous penetrating cracks (Fig. 3(e)), which were absent in the pure YSZ coating (Fig. 3(a)). These cracks act as rapid oxygen diffusion channels, accelerating TGO growth. These results indicate that penetrating vertical cracks are the primary cause of failure in the RSZ/YSZ coatings under thermal cycling at 1130 °C.

3.3 Thermal shock lifespan at 1600 °C

Figure 4 compares the thermal shock lifespans of the five types of coatings at 1600 °C. Consistent with its superior thermal cycling resistance (Fig. 3), the RSZ/YSZ coating resulted in the longest thermal shock lifespan. The pure RSZ coating also performed well, surviving 10 cycles—more than most other candidates. Among the remaining systems, GZO/YSZ exhibited the best thermal shock durability. The coating with 100 μm YSZ and 400 μm GZO reached 12 cycles at 1400 °C [36]. In contrast, the LZO/YSZ coating underwent only 6 cycles because of its low fracture toughness and thermal expansion coefficient (Table 2). This observation is consistent with reports that an LZO/YSZ coating with 200 μm YSZ and 201 μm LZO survived 9 cycles at 1300 °C, whereas another with 100 μm YSZ and 268 μm LZO failed after only 2 cycles at 1300 °C [15]. The GTO/YSZ coatings resulted in the shortest lifespan (5 cycles) at 1600 °C [2], which is consistent with the low thermal expansion coefficient of GTO (Table 2). The pure YSZ coating performed poorly under these conditions, failing in less than 90 s at 1600 °C and surviving only 2 cycles at 1550 °C [2]. This contrasts sharply with its reported lifespan of

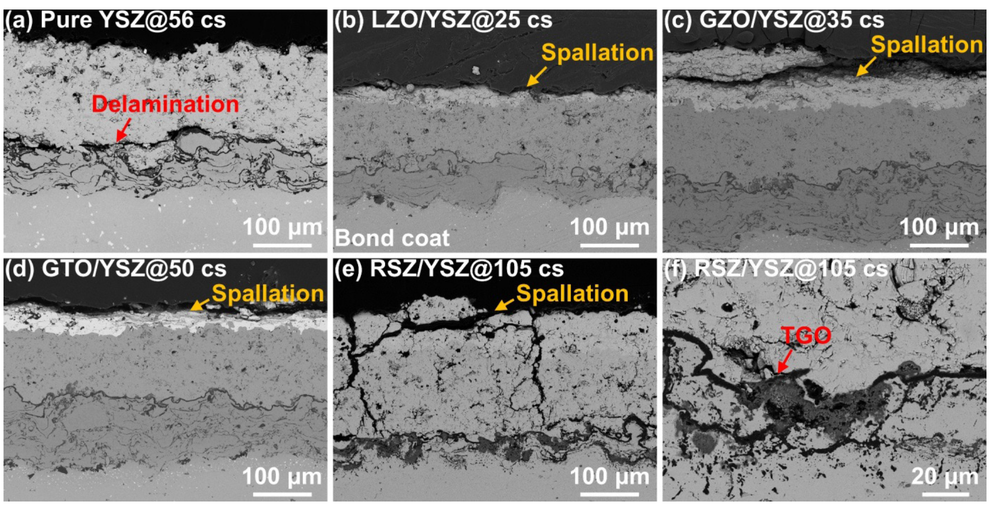

Fig. 3 Cross-sectional microstructures of TBCs after thermal cycling tests at 1130 °C: (a) pure YSZ, (b) LZO/YSZ, (c) GZO/YSZ, (d) GTO/YSZ, and (e, f) RSZ/YSZ. The symbol cs is an abbreviation for cycles.

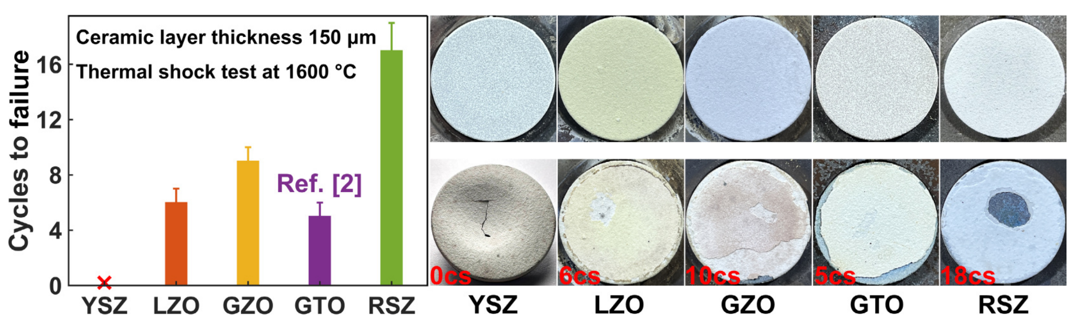

Fig. 4 Thermal shock lifespan of TBCs with a ceramic layer thickness of 150 μm at 1600 °C. Thicknesses of LZO, GZO, GTO, and RSZ topcoats were maintained at 60 μm.

91 cycles at 1300 °C for a 500 μm coating [15,37], indicating a fundamental change in the failure mechanism above 1600 °C. The pure YSZ sample exhibited significant depression deformation, suggest pronounced substrate softening at this temperature. In contrast, all the DCL coatings ultimately failed by topcoating or full ceramic layer spallation, underscoring the protective role of the DCL structure under extreme thermal shock.

Figure 5 shows the coating microstructures after thermal shock testing at 1600 °C. In the pure YSZ coating, extensive void formation occurred at the BC/YSZ interface (Fig. 5(a)), which is consistent with the macroscopic deformation in Fig. 4. Similar to the behavior at 1130 °C (Figs. 3(b) and 3(c)), severe topcoat spallation was observed in the LZO/YSZ and GZO/YSZ coatings (Figs. 5(b) and 5(c)), indicating that LZO and GZO are unsuitable for rocket engine applications. The GTO/YSZ coating failed at the BC/YSZ interface (Fig. 5(d)), which is consistent with its moderate fracture toughness (Table 2). In the RSZ/YSZ coating, spallation occurred both within the RSZ topcoat and at the BC/YSZ interface (Fig. 5(e)). Noticeable sintering of the RSZ coating was observed above the transverse cracks (Fig. 5(f)), which was supported by a sharp hardness increase from 421 to 955 HV. Similar sintering has been reported for YSZ [38], LCO [39,40], LCO/YSZ [41], and LZO/YSZ [15] coatings tested at 1150–1350 °C. These results confirm that sintering-induced spallation is the dominant failure mechanism for the RSZ/YSZ coatings at 1600 °C.

Additionally, multiple reaction products were detected on the surfaces of the LZO/YSZ, GZO/YSZ, and GTO/YSZ coatings. Diffraction peaks corresponding to $CaSiO_3$ were identified on the LZO/YSZ and GZO/YSZ coatings (Figs. 6(a) and 6(b)), whereas $Ca_2Ta_2O_7$ was detected on the GTO/YSZ coatings [2]. The presence of calcium and silicon is attributed mainly to cooling water impurities, as confirmed by the scale on the fixture backside. These products reflect the poor structural stability of these materials at 1600 °C. In contrast, no reaction products were found on the RSZ/YSZ coatings (Fig. 6(c)), demonstrating their superior overall performance and potential for rocket engine applications.

3.4 Thermal shock lifespan at 1800 °C

Both thermal cycling tests at 1130 °C and thermal shock tests at 1600 °C confirm the superior performance of RSZ/YSZ coatings, underscoring their potential for rocket engines. Since 1600 °C is only a baseline surface temperature and the ultimate target is 1900 °C, the total ceramic layer thickness and YSZ-to-RSZ thickness ratio were further optimized to achieve a target lifespan of 15 cycles under these extreme conditions.

First, the ceramic layer thickness was optimized at a fixed YSZ-to-RSZ ratio of 3 : 2. When the total thickness exceeds 375 μm, the bond strength decreases below 20 MPa (although it remains above 15 MPa). The thermal cycling lifetimes at 1130 °C were 90, 95, 74, and 65 cycles for thicknesses of 275, 325, 375, and 425 μm, respectively. These values were above the minimum requirement of 30 cycles and were superior to those of other alternatives (Fig. 2). Figure 7(a) shows the variation in the thermal shock lifespan with increasing ceramic thickness at 1800 °C. Coatings with thicknesses of 325 and 425 μm achieve 12 and 14 cycles, respectively. Although the 425 μm coating had a longer thermal shock lifespan, it presented a lower bond strength and reduced thermal cycling durability, suggesting that a thickness around 325 μm offers the best overall performance.

Figure 8 shows photographs of thermally shocked samples with various ceramic thicknesses. With increasing thickness, distinct changes in the failure modes were observed. Below 325 μm, failure is dominated by substrate warping (Figs. 8(a) and 8(b)), without macroscopic coating spallation. The noticeable deformation indicates significant substrate softening at 1800 °C, as evidenced by the rapid failure of the pure YSZ coatings (Fig. 4). Above 375 μm, macroscopic mud cracking and localized spallation occur (Figs. 8(c) and 8(d)). A positive correlation exists between the thermal shock lifespan and the time at which visible mud cracks first appear. These results suggest that a ceramic thickness near 350 μm may offer optimal thermal shock resistance at 1800 °C.

Figure 9 shows the microstructures of the coatings with various thicknesses after thermal shock testing at 1800 °C. After 5 cycles, all the samples exhibited periodic vertical cracks, mostly terminating within the YSZ interlayer. The crack densities were 10.1±0.7 cm^{-1} (275 μm), 5.0±0.4 cm^{-1} (325 μm), 13.4±0.6 cm^{-1} (375 μm), and 10.6±0.8 cm^{-1} (425 μm), indicating that the 325 μm coating offers the best resistance to channel cracking. In the final state, although macroscopic photographs revealed no coating spallation (Figs. 8(a) and 8(b)), coatings thinner than 325 μm showed severe spallation at the BC/YSZ interface (Figs. 9(a2) and 9(b2)). Significant grain growth and coating densification were observed on the surface (Figs. 9(a3) and 9(b3)), indicating rapid sintering at 1800 °C. Rapid sintering has also been observed in YSZ [38], LCO [39,40], LCO/YSZ [41], and LZO/YSZ [15,42]

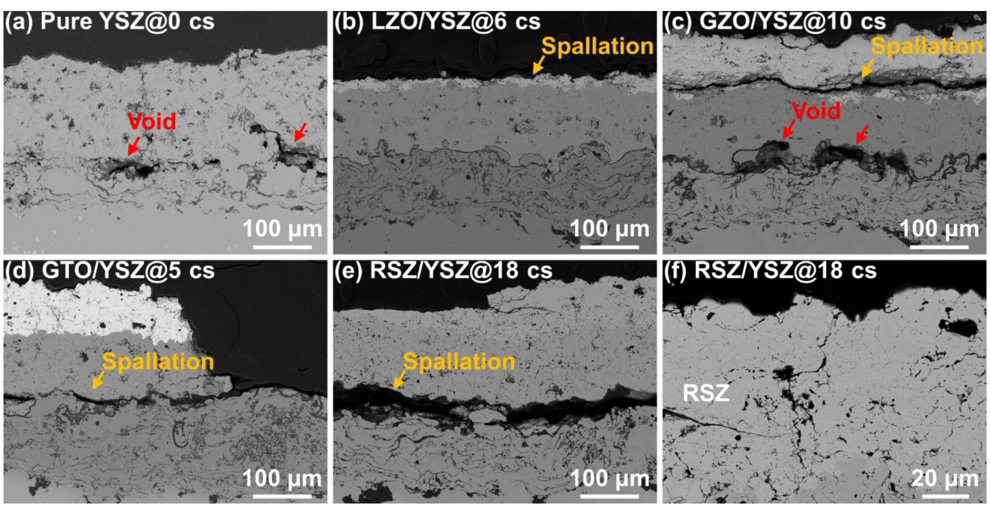

Fig. 5 Cross-sectional microstructures of DCL TBCs after thermal shock tests at 1600 °C: (a) pure YSZ, (b) LZO/YSZ, (c) GZO/YSZ, (d) GTO/YSZ, and (e, f) RSZ/YSZ. Ceramic layer thickness of DCL TBCs was 150 μm.

https://doi.org/10.26599/JAC.2025.9221228

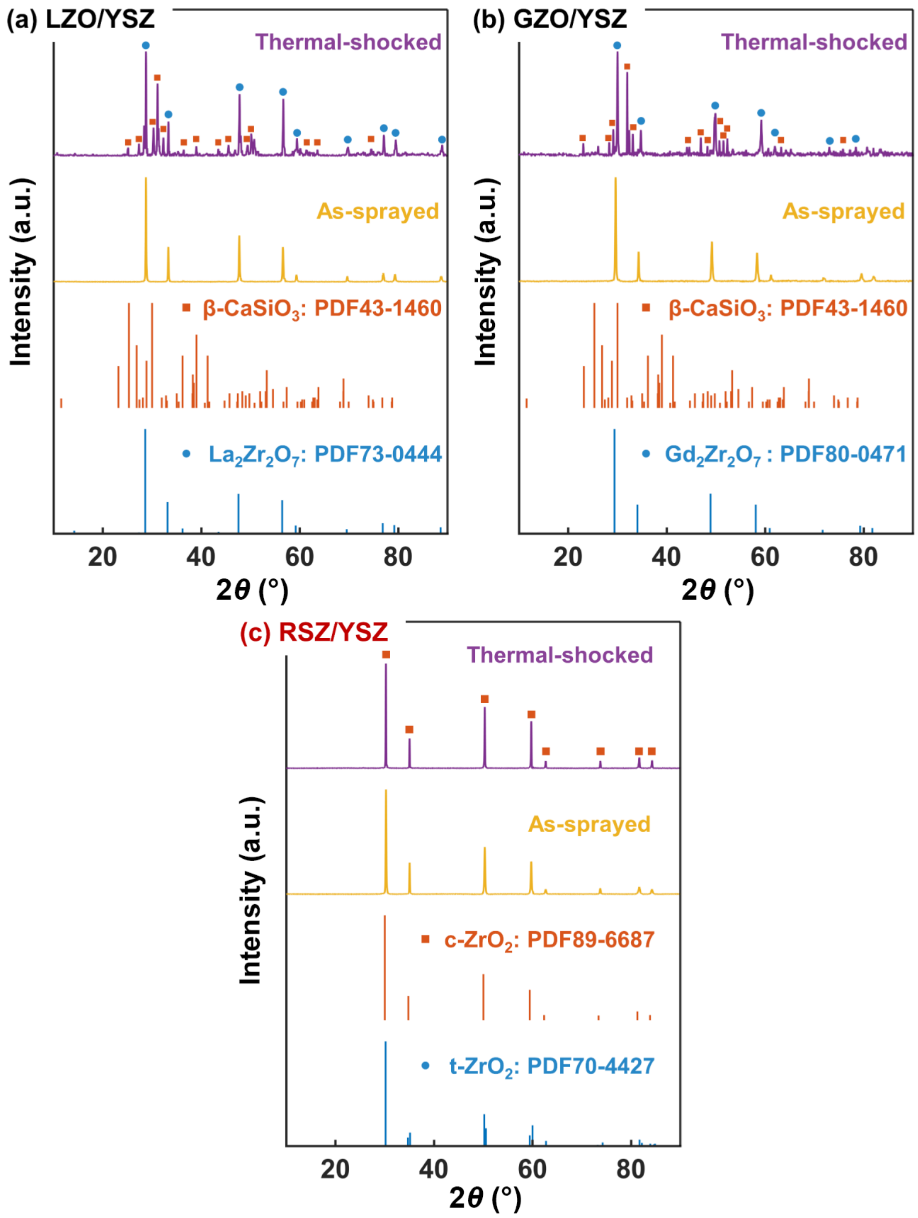

Fig. 6 XRD patterns of (a) LZO/YSZ, (b) GZO/YSZ, and (c) RSZ/YSZ coatings after thermal shock at 1600 °C.

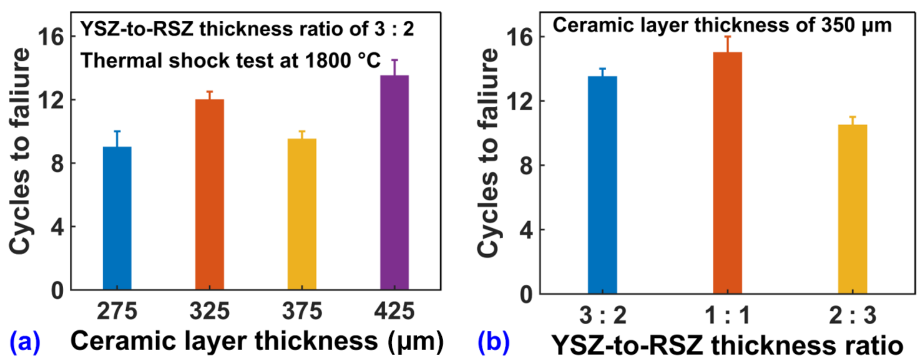

Fig. 7 Thermal shock lifespan of RSZ/YSZ coatings at 1800 °C: (a) with varying ceramic layer thicknesses and (b) with varying YSZ-to-RSZ thickness ratios.

coatings tested at 1150–1350 °C. For thicknesses above 375 μm, interconnected mud cracks appeared (Figs. 9(c3) and 9(d3)). Compared with the 425 μm coating, the 375 μm coating developed wider mud cracks, which can be attributed to more severe BC/YSZ interface spallation (Figs. 9(c2) and 9(d2)). Consequently, the former demonstrates a shorter lifespan (Fig. 8(a)). All the samples had TGO thicknesses less than 3 μm, which is less than the critical 5–6 μm [25], confirming that TGO growth is not the dominant failure mechanism. These results collectively demonstrate that RSZ/YSZ coatings with thicknesses of 325 and 425 μm provide superior thermal shock resistance at 1800 °C.

To further increase the thermal shock lifespan at 1800 °C, the

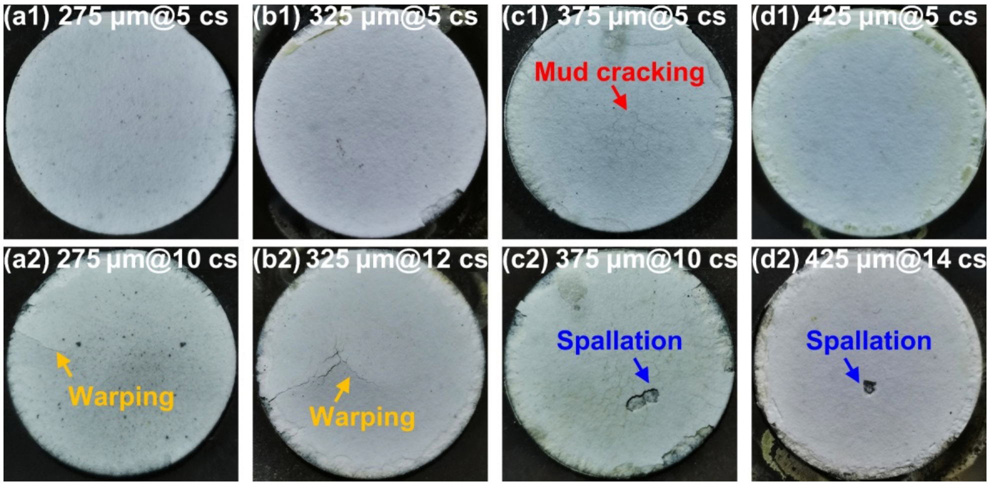

Fig. 8 Photographs of thermally shocked samples with varying ceramic layer thicknesses: (a) 275 μm, (b) 325 μm, (c) 375 μm, and (d) 425 μm. YSZ-to-RSZ thickness ratio was maintained at 3 : 2.

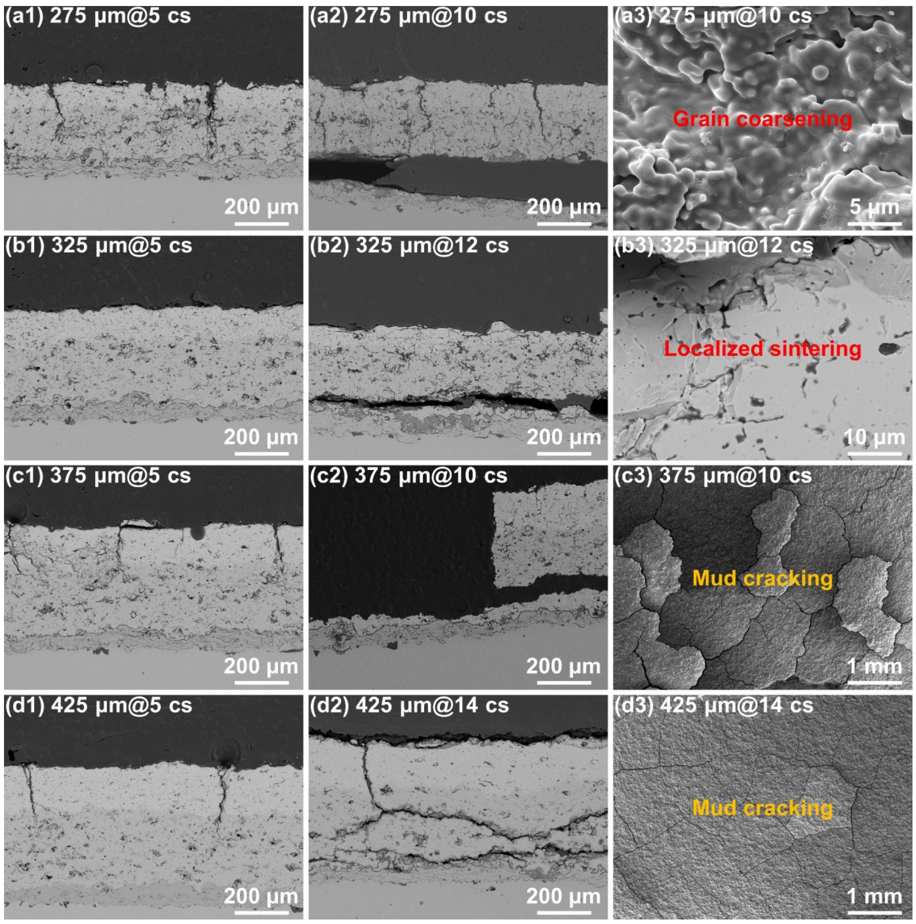

Fig. 9 Microstructures of RSZ/YSZ DCL coatings after thermal shock tests at 1800 °C with various ceramic layer thicknesses: (a) 275 μm, (b) 325 μm, (c) 375 μm, and (d) 425 μm. YSZ-to-RSZ thickness ratio was maintained at 3 : 2.

YSZ-to-RSZ thickness ratio was optimized. The total ceramic layer thickness was maintained at 350 μm, where the bond strength remained above 20 MPa. At this thickness, the thermal cycling lifetimes at 1130 °C were 100, 74, and 36 cycles for YSZ-to-RSZ ratios of 3 : 2, 1 : 1, and 2 : 3, respectively. All values exceed the minimum lifespan requirement for typical rocket engines. Figure 7(b) shows the variation in the thermal shock lifespan with the YSZ-to-RSZ ratio at 1800 °C. A 1 : 1 ratio sample achieved an average lifespan of 15 cycles, meeting the performance benchmark for rocket engines under such extreme temperatures. These results confirm that the RSZ/YSZ coating with a 350 μm thickness and a 1 : 1 ratio offers superior thermal shock resistance at 1800 °C.

Figure 10 shows the cross-sectional microstructures of the 350 μm RSZ/YSZ coatings after testing at 1800 °C at different ratios. After five cycles, all the samples exhibited periodic vertical cracks. The crack densities were 14.1±0.7 cm^{-1} (3 : 2),

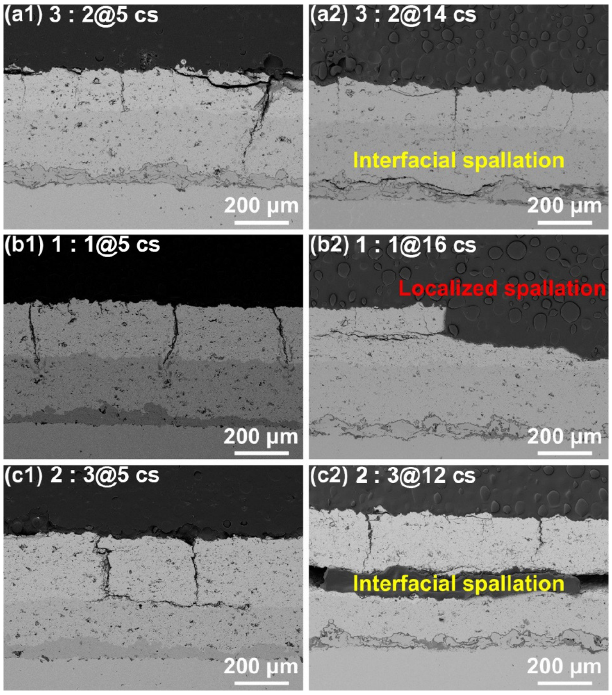

Fig. 10 Cross-sectional microstructures of RSZ/YSZ DCL coatings after thermal shock tests at 1800 °C, with varying YSZ-to-RSZ thickness ratios: (a) 3 : 2, (b) 1 : 1, and (c) 2 : 3. Total ceramic layer thickness was maintained at 350 μm.

13.2±0.6 cm^{-1} (1 : 1), and 12.7±0.4 cm^{-1} (2 : 3). Additionally, spallation occurred within the RSZ topcoat in the 3 : 2 sample (Fig. 10(a1)) and at the RSZ/YSZ interface in the 2 : 3 sample (Fig. 10(c1)). In contrast, the 1 : 1 sample formed additional vertical cracks without spallation (Fig. 10(b1)). In the final state, failure in the 3 : 2 sample occurred mainly at the BC/YSZ interface (Fig. 10(a2)), whereas failure in the 2 : 3 sample occurred at the RSZ/YSZ interface (Fig. 10(c2)). The 1 : 1 sample exhibited only localized RSZ topcoat spallation (Fig. 10(b2)). This localized spallation correlates with its superior thermal shock performance (Fig. 7(b)). Comparisons with other systems show that the optimal thickness ratio strongly depends on the temperature and material. For example, RSZ/YSZ with a 1 : 2 ratio and 180 μm thickness performs best at 1600 °C [43]. LGYYSZ/YSZ with a 2 : 3 ratio and 500 μm thickness demonstrated optimal resistance at 1400 °C [16]. GZO/YSZ coatings with a 1 : 4 ratio and 500 μm thickness excel at 1400 °C [44,45]. Yb-LZO/YSZ with a 3 : 2 ratio and 500 μm thickness performs best at 1050 °C [19]. These comparisons highlight that the coating lifetime is strongly influenced by the ceramic layer thickness, thickness ratio, service temperature, and topcoat material. Among all the tested configurations, the RSZ/YSZ coating with a thickness of 350 μm and a 1 : 1 ratio provides the best thermal shock performance at 1800 °C.

3.5 Temperature dependence of the thermal shock lifespan

The coating with a ceramic thickness of 325 μm and a thickness

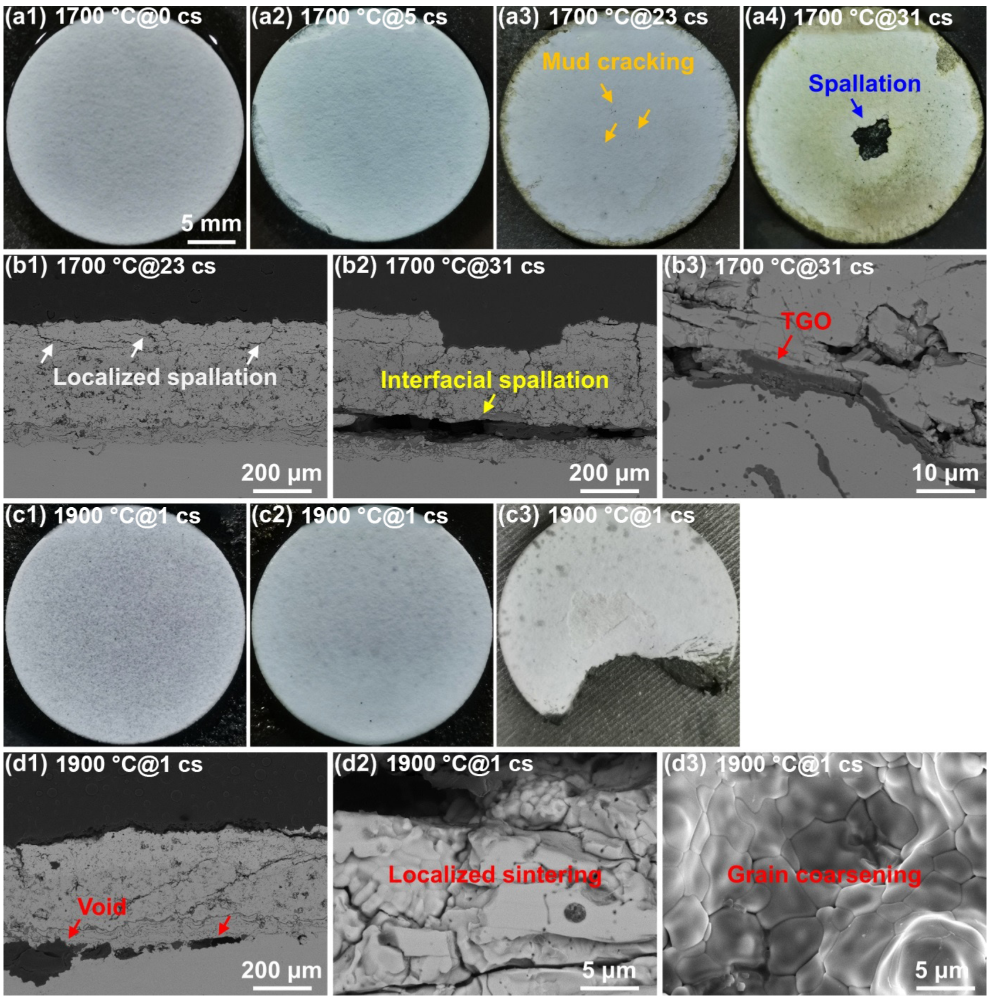

Fig. 11 Photographs and microstructures of samples thermally shocked at (a, b) 1700 °C and (c, d) 1900 °C. Total ceramic layer thickness and YSZ-to-RSZ thickness ratio were maintained at 325 μm and 3 : 2, respectively.

ratio of 3 : 2 achieved a thermal shock lifespan of 31 cycles at 1700 °C (Fig. 11(a)), significantly surpassing its performance at 1800 °C. In contrast, the lifespan decreased sharply to only one cycle at 1900 °C (Fig. 11(c)), underscoring the substantial impact of temperature on coating durability. A similar trend has been observed in pure YSZ coatings at lower temperatures [38,46]. During testing at 1700 °C, visible cracks and spallation were observed at the sample center after 23 and 31 cycles, respectively. The final failure at this temperature was dominated by spallation at the BC/YSZ interface, occurring mainly beneath regions where the RSZ layer had already spalled (Fig. 11(b2)). The samples maintained a TGO thickness below 5 μm, indicating that TGO growth was not the primary failure mechanism under these conditions. At 1900 °C, however, voids formed at the BC/YSZ interface (Fig. 11(d1)), similar to those observed in pure YSZ coatings (Fig. 5(a)), indicating significant substrate softening. Substantial grain coarsening was also observed on the coating surface (Fig. 11(d3)), reflecting extremely rapid sintering at this temperature. These results indicate that failure at 1900 °C is governed by pronounced sintering-induced substrate softening, underscoring the need for novel structural design strategies to achieve extended lifetimes under such extreme thermal conditions.

3.6 Reflectance of DCL TBCs

A key finding is that even a thin layer of alternative topcoat materials can significantly enhance the thermal shock resistance of YSZ coatings (Fig. 4). Although DCL coatings show only minor differences in thermal conductivity and fracture toughness compared with those of pure YSZ (Table 2), their thermal cycling performance is markedly superior. For example, at 1600 °C, pure YSZ failed at 90 s, whereas the RSZ/YSZ coating survived 18 full cycles (Fig. 4). Similarly, at 1550 °C, pure YSZ failed in the second cycle, but the GTO/YSZ coating lasted 15 cycles [2].

The main difference between YSZ and other candidate materials is their reflectance (Fig. 12). YSZ is partially transparent to infrared radiation below 5 μm [32] and has a reflectance of 35% within the 1.0–2.2 μm range [47]. As a result, a considerable fraction of incident thermal radiation penetrates the pure YSZ coating and is absorbed by the underlying substrate, leading to pronounced depression deformation (Fig. 4) and interfacial void formation (Fig. 5(a)). In contrast, a highly reflective topcoat effectively attenuates radiative heat transfer to the substrate. This explanation is consistent with the observed failure mode of DCL TBCs, which is dominated by topcoat spallation rather than substrate deformation (Figs. 4 and 5). In support of this, an increase in reflectance from 35% to 45% has been shown to reduce the thermal conductivity of electron beam physically vapor-deposited YSZ from 1.8 to 1.2 W·m^{-1}·K^{-1} at 1316 °C [47]. These findings demonstrate that DCL TBCs are a highly suitable choice for rocket engine applications where operating temperatures exceed 1600 °C.

4 Discussion

4.1 BC softening under thermal shock

Without considering the contribution of radiative heat transfer, the temperature at the BC/YSZ interface during thermal shock (T_{BC}) can be expressed as Eq. (1):

$$T_{BC} = \frac{\frac{h_1}{\kappa_1}T_0 + \frac{h}{1+\lambda}\left(\frac{1}{\kappa_3}+\frac{\lambda}{\kappa_2}\right)T_1}{\frac{h_1}{\kappa_1} + \frac{h}{1+\lambda}\left(\frac{1}{\kappa_3}+\frac{\lambda}{\kappa_2}\right)} \tag{1}$$

where T_0 and T_1 represent the temperatures of the coating surface (1600–1800 °C) and the substrate back surface (600 °C), respectively; h_1 and h denote the thicknesses of the substrate and ceramic layer, respectively; λ is the YSZ-to-RSZ thickness ratio; κ_1, κ_2, and κ_3 indicate the thermal conductivities of the substrate, YSZ intermediate layer, and RSZ topcoat, respectively.

Figure 13 shows the predicted temperature at the BC/YSZ interface during thermal shock at 1800 °C. Coatings with higher interface temperatures generally exhibit shorter thermal shock lifespans (Fig. 13(b)). However, the coating with the lowest interface temperature does not exhibit a superior lifespan. These results suggest that the interface temperature is not the sole factor governing the thermal shock performance.

In this study, the temperature of the BC exceeded 0.8 times the melting point of the Ni-based superalloy. Under such conditions, creep is governed by Nabarro–Herring diffusion, and the tensile creep rate ($\dot{\varepsilon}_{NH}$) is expressed as Eq. (2):

$$\dot{\varepsilon}_{NH} = A_{NH}\frac{\Omega\sigma}{d^2kT_{BC}}D_0\exp\left(-\frac{Q_d}{RT_{BC}}\right) \tag{2}$$

where D_0 is the coefficient for lattice self-diffusion, Ω is the atomic volume, d is the grain size, k is Boltzmann's constant, R is the gas constant, Q_d is the diffusion activation energy, and A_{NH} is a constant.

Using typical parameter values, Fig. 13(c) shows the variation in the creep rate with increasing BC temperature, highlighting its high-temperature sensitivity. A power-law fit yields Eq. (3):

$$\dot{\varepsilon}_{NH} = 0.015\left[T_{BC}/\left(\frac{T_0+T_1}{2}\right)\right]^{23.6} \tag{3}$$

where the BC temperature can be approximated as Eq. (4):

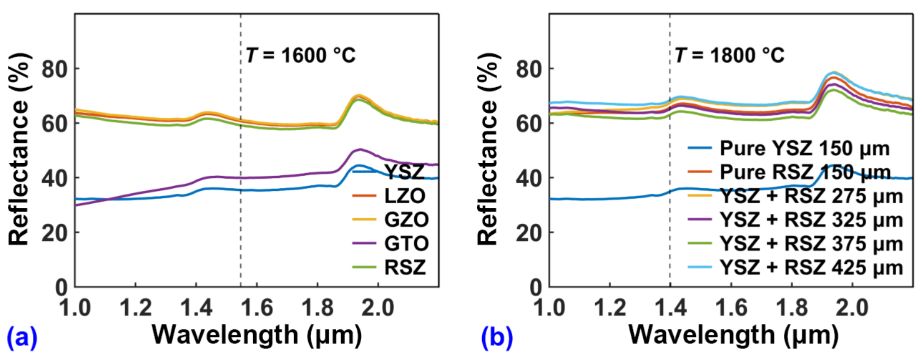

Fig. 12 Reflectance of DCL TBCs: (a) ceramic layer thickness of 150 μm and (b) varying ceramic layer thickness. Dotted lines indicate the blackbody emission peaks corresponding to temperatures of 1600 and 1800 °C.

$$T_{BC}=\frac{T_0+T_1}{2}\left[1-0.123\cdot\left(\frac{\kappa_3}{\kappa_2}\right)^{-0.59}\right] \tag{4}$$

These results indicate that the thermal conductivity of the topcoat significantly influences BC softening.

4.2 Energy release rates of the RSZ/YSZ TBCs under thermal shock

According to the predicted temperature shown in Fig. 13, the energy release rate governing coating spallation is given by Eq. (5) [48]:

$$G=-\frac{1}{2}\frac{\partial}{\partial a}\iiint_{\Omega}\sigma_{ij}\varepsilon_{ij}\mathrm{d}V \tag{5}$$

where σ_{ij} and ε_{ij} represent the stress and strain components in the system, respectively. a is the crack length. Assuming that the film-substrate system is elastically homogeneous and that the substrate is semi-infinite, the energy release rate for steady-state interfacial spallation can be approximated as Eq. (6) [48]:

$$G=\frac{\sigma^2 h}{2\bar{E}_f} \tag{6}$$

where σ and $\bar{E}_f$ represent the applied stress and plane-strain modulus of the ceramic layer, respectively.

However, this analytical model does not fully apply under the present thermal shock conditions because of the gradient stress distribution within the ceramic layer [49], which induces a bending moment. Additionally, compressive stress develops within the YSZ layer near the substrate, contributing to crack arrest within this layer during 1800 °C thermal shock.

Figure 14 shows the calculated energy release rate for the RSZ/YSZ coating. In this study, the elastic moduli of the RSZ and YSZ coatings were measured via the Knoop indentation method with a load of 2.94 N and a holding time of 30 s. The measured values are approximately 25±8 GPa, comparable to those of the LCO [39] and GZO [34] coatings. In contrast to the analytical solution in Eq. (6), the energy release rate has a power-law relationship with ceramic thickness (Fig. 14(a)), underscoring the significant impact of the bending moment. Furthermore, for the 350 μm coating, the energy release rates at the BC/YSZ and RSZ/YSZ interfaces are similar when the YSZ-to-RSZ ratio is less than 1.0 (Fig. 14(b)). This means that the thickness ratio significantly influences the spall location. These findings suggest that both the ceramic thickness and thickness ratio critically affect coating spall.

Figure 15 shows a map of the energy release rates. The values are close to those of GZO/YSZ coatings with a 600 μm thickness and a 0.5 ratio [8]. Using a thinner ceramic layer or a lower YSZ-to-RSZ ratio reduces the spall risk. However, it also increases the BC temperature (Fig. 13(a)). Therefore, a balanced design of

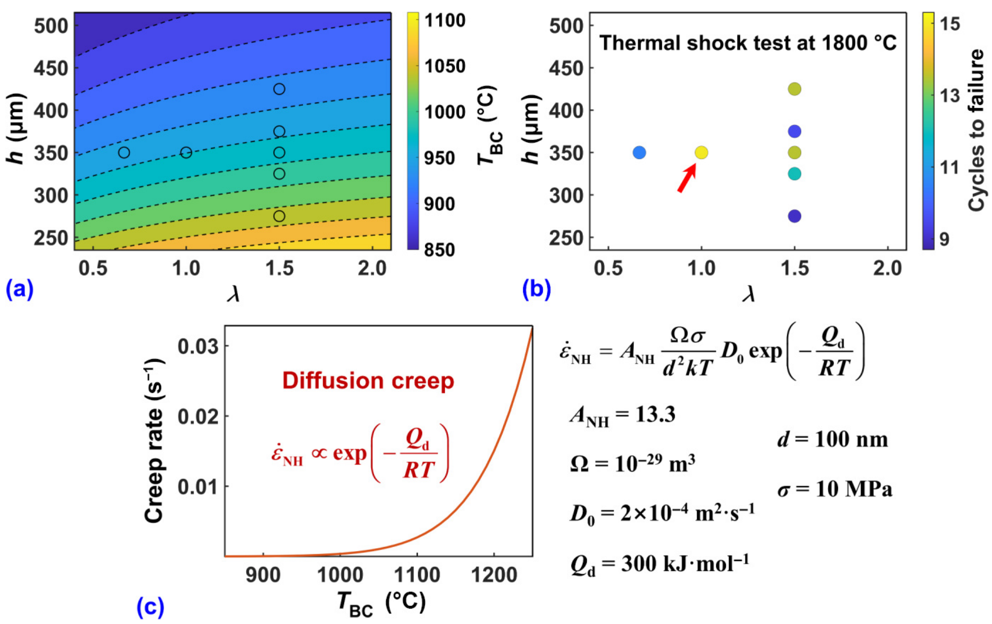

Fig. 13 (a) Predicted BC/YSZ interface temperature during thermal shock at 1800 °C, (b) corresponding thermal shock lifespan of RSZ/YSZ DCL coatings, and (c) creep rate with increasing BC/YSZ interface temperature.

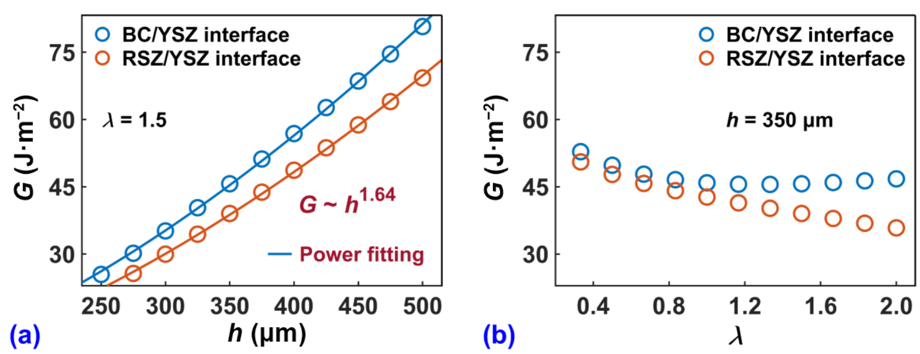

Fig. 14 Energy release rates for RSZ/YSZ DCL coating spallation: (a) with varying ceramic thicknesses and (b) with varying YSZ-to-RSZ thickness ratios.

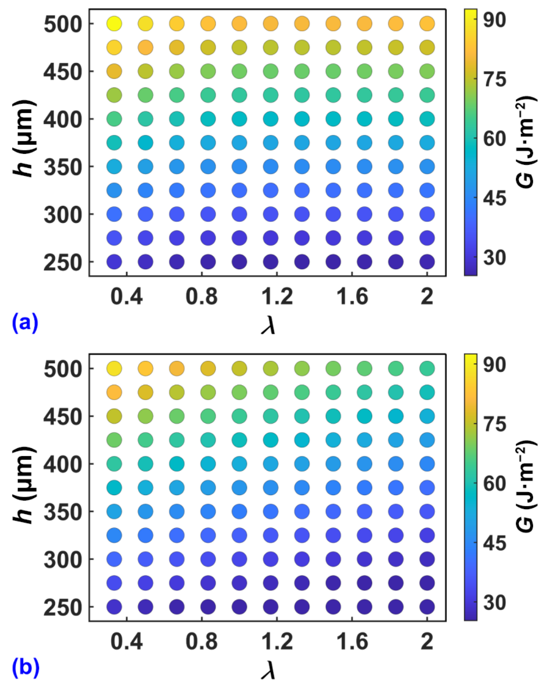

Fig. 15 Energy release rate map for RSZ/YSZ DCL coating spallation: (a) at BC/YSZ interface and (b) at RSZ/YSZ interface.

ceramic thickness and thickness ratio is essential to simultaneously achieve low BC temperatures and low energy release rates.

4.3 Failure mechanisms of the RSZ/YSZ DCL TBCs under thermal shock

Figure 16 summarizes how the RSZ/YSZ coatings fail under thermal shock. For coatings with a thin ceramic layer, the BC and substrate become too hot and soft. Spallation occurs early at the BC/YSZ interface (Fig. 16(a)). For coatings with a thick ceramic layer but a large YSZ-to-RSZ ratio (i.e., a thin RSZ topcoat), a high energy release rate causes spallation at the BC/YSZ interface (Fig. 16(b)). For coatings with a thick ceramic layer and a small ratio (i.e., a thick RSZ topcoat), a high energy release rate causes spallation at both the BC/YSZ and RSZ/YSZ interfaces (Fig. 16(c)). In contrast, a moderate ceramic thickness and thickness ratio minimize both the BC temperature and energy release rate (Fig. 16(d)), leading to a failure mode dominated by sintering-induced localized spallation (Figs. 9(b3) and 10(b2)). Unlike mechanically driven rapid cracking (Figs. 14(b) and 14(c)), coating sintering is a thermally activated diffusion-controlled process that proceeds more slowly and helps extend the coating lifespan. These findings emphasize that carefully choosing the thickness and ratio is key to maximizing the thermal shock lifespan of DCL TBCs.

4.4 RSZ topcoats with superior overall performance

A significant finding is that both the BC temperature and energy release rate substantially influence the thermal shock lifespan of TBCs. Elevated BC temperatures cause substrate softening and warping, leading to premature failure (Fig. 16(a)), as evidenced by the fast failure of pure YSZ at 1600 °C (Fig. 4). Therefore, a topcoat with lower thermal conductivity and greater thickness is expected to reduce the BC temperature. However, thicker coatings increase the energy release rate (Fig. 14(a)), which can induce premature spallation (Figs. 16(b) and 16(c)). To address this issue, a topcoat with higher fracture toughness and a greater thermal expansion coefficient is needed. Moreover, to handle high radiative heat above 1600 °C, a topcoat must be more reflective (less transparent). Thus, an ideal topcoat for maximizing thermal shock resistance should combine low thermal conductivity, high fracture toughness, a high thermal expansion coefficient, and high reflectance. Although RSZ topcoats do not excel in any single property, they distinguish themselves by offering an optimal balance of these key characteristics (Table 2). This well-rounded performance makes RSZ-based TBCs particularly suitable for reusable rocket engines.

In this study, a dimensionless analysis was conducted to determine the dominant factor for the thermal shock lifespan. The lifespan can be expressed as Eq. (7):

$$\Pi = \Pi_1 \cdot \Pi_2 \tag{7}$$

where Π_1 and Π_2 represent the contributions from BC softening and thermal mismatch stress-induced spalling, respectively.

Softening-induced failure is proportional to the reciprocal of the creep rate (Eq. (8)):

$$\Pi_1 = f_1\left(\frac{1}{\dot{\varepsilon}_{\mathrm{NH}}}\right) \tag{8}$$

where f_1 denotes a function symbol.

For typical values of κ_3/κ_2 ranging from 0.3 to 1.2, in combination with Eqs. (3) and (4), the reciprocal of the creep rate can be expressed as Eq. (9):

$$\frac{1}{\dot{\varepsilon}_{\mathrm{NH}}} = 832\left(\frac{\kappa_3}{\kappa_2}\right)^{-3.4} \tag{9}$$

Thus, considering the contributions of heat radiative flux, the lifespan related to BC softening can be expressed as Eq. (10):

$$\Pi_1 = f_2\left(\left(\frac{1}{1-\eta}\cdot\frac{\kappa_2}{\kappa_3}\right)^{3.4}\right) \tag{10}$$

where η represents the reflectance of the coating (Fig. 12).

The dimensionless driving force for coating spallation is given by Eq. (11)[48]:

$$\Pi_2 = f_3\left(\frac{K_{\mathrm{IC}}}{E\Delta\alpha\Delta T\sqrt{h}}\right) \tag{11}$$

where $\Delta\alpha$ is the thermal expansion coefficient mismatch between the coating and the substrate, and K_{IC} represents the fracture toughness of the coating. The coefficients E and ΔT denote the coating modulus and temperature difference between the coating and the substrate, respectively.

Therefore, to characterize the lifespan of DCL TBCs under thermal shock conditions, a compatibility factor (ϑ) is defined as Eq. (12):

$$\vartheta = \left(\frac{1}{1-\eta}\cdot\frac{\kappa_2}{\kappa_3}\right)^{3.4}\cdot\frac{K_{\mathrm{IC}}}{E\Delta\alpha\Delta T\sqrt{h}} \tag{12}$$

where η represents the reflectance of the coating (Fig. 12).

The compatibility factor is particularly applicable to DCL TBCs used in rocket engines operating at temperatures exceeding 1600 °C. According to the data presented in Table 2, the calculated values confirm that the RSZ topcoat exhibits superior overall performance (Fig. 17(a)), which is consistent with the thermal shock lifespan of DCL TBCs at 1600 °C (Fig. 17(b)). These findings indicate that optimizing the overall performance of topcoats is essential for increasing the lifespan of TBCs under extreme thermal shock in rocket engine applications.

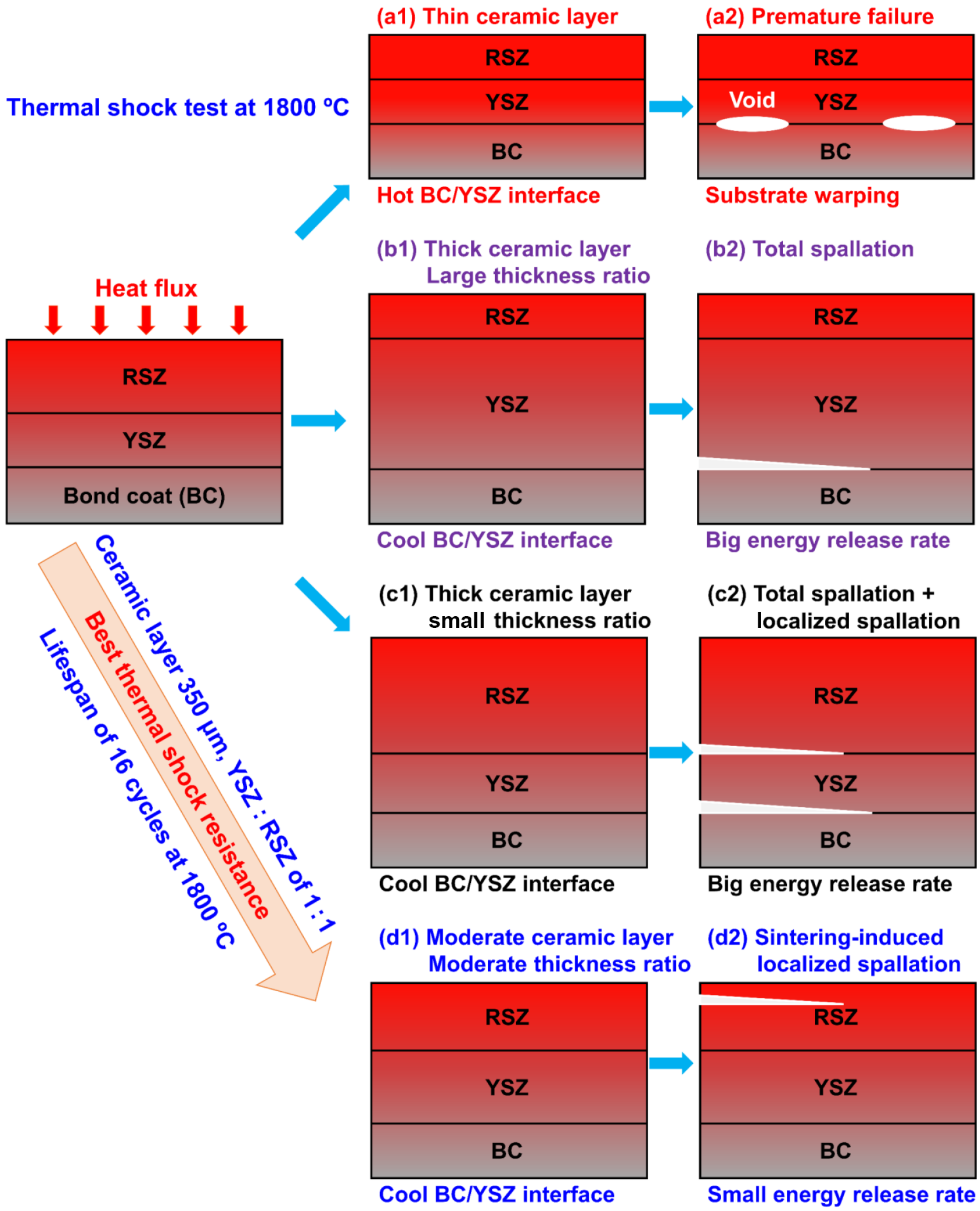

Fig. 16 Schematic illustration of failure mechanisms in RSZ/YSZ DCL TBCs with varying ceramic layer thicknesses and YSZ-to-RSZ thickness ratios under thermal shock tests at 1800 °C.

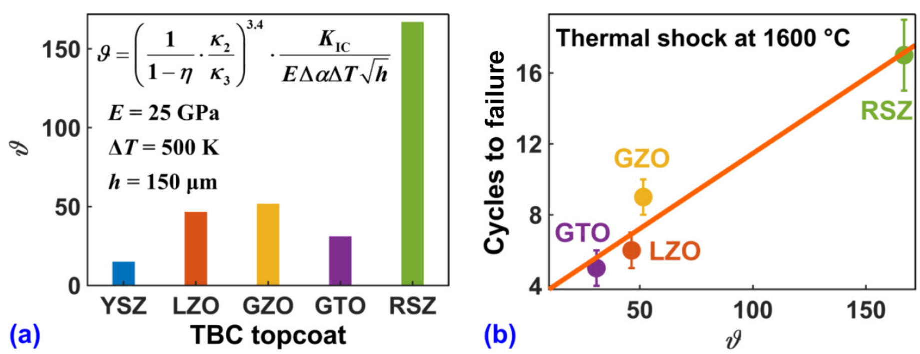

Fig. 17 Compatibility factor for evaluating the (a) overall performance of TBC topcoats and (b) corresponding thermal shock lifespan at 1600 °C.

5 Conclusions

TBCs capable of withstanding temperatures up to 1800 °C for extended durations are critical to the development of advanced rocket engines. However, conventional YSZ coatings fail quickly above 1600 °C, and TBCs commonly employed in aeroengines and gas turbines also fail to meet the requirements under such extreme conditions. To overcome these limitations, this study developed a novel quaternary RSZ material and systematically optimized the architecture of RSZ/YSZ DCL TBCs. A comprehensive investigation into their failure mechanisms under extreme thermal exposure yielded the following conclusions:

(1) Compared with other candidate coatings, the RSZ topcoat demonstrates superior overall performance, enabling RSZ/YSZ TBCs to achieve significantly extended lifespans under both thermal cycling at 1130 °C and thermal shock at 1600 °C.

(2) An optimized RSZ/YSZ coating configuration—with a total ceramic thickness of 350 μm and a YSZ-to-RSZ thickness ratio of 1 : 1—demonstrated excellent thermal shock resistance at 1800 °C. It achieves a lifespan of 15 cycles, which satisfies the performance benchmark for rocket engines under such extreme temperatures.

(3) Coating failure transitions to interfacial spall when the ceramic layer is overly thick or the YSZ-to-RSZ ratio is insufficient. Therefore, careful control of the thickness and ratio is essential to maximize the thermal shock resistance at 1800 °C. Under the optimized configuration, failure occurs by sintering-induced localized spallation—a relatively slow process that contributes to extended coating durability.

Acknowledgements

The present project is supported by the National Natural Science Foundation of China (No. 52401109).

Availability of data and materials

The data that support the findings of this study are available from the corresponding author upon reasonable request.

Competing interests

The authors declare that they have no known competing financial interests or personal relationships that could have appeared to influence the work reported in this paper. The author Guan-Jun Yang is the Editorial Committee member of this journal.

References

[1] Zhou C, Yu NJ, Wang SW, *et al.* The influence of thrust chamber structure parameters on regenerative cooling effect with hydrogen peroxide as coolant in liquid rocket engines. *Aerospace* 2023, **10**: 65.

[2] Xie ZL, Li C, Zhang HX, *et al.* Durable $GdTaO_4$/YSZ double-ceramic-layer thermal barrier coatings against ultrahigh-temperature thermal shock. *Ceram Int* 2025, **51**: 29781–29791.

[3] Fagherazzi M, Santi M, Barato F, *et al.* A simplified thermal analysis model for regeneratively cooled rocket engine thrust chambers and its calibration with experimental data. *Aerospace* 2023, **10**: 403.

[4] Seedhouse E. Starship to Mars–The First 20 Years. Germany: Praxis Cham, 2022.

[5] Vaßen R, Bakan E, Mack DE, *et al.* A perspective on thermally sprayed thermal barrier coatings: Current status and trends. *J Therm Spray Techn* 2022, **31**: 685–698.

[6] Vaßen R, Mack DE, Tandler M, *et al.* Unique performance of thermal barrier coatings made of yttria-stabilized zirconia at extreme temperatures (> 1500 °C). *J Am Ceram Soc* 2021, **104**: 463–471.

[7] Zhou DP, Mack DE, Bakan E, *et al.* Thermal cycling performances of multilayered yttria-stabilized zirconia/gadolinium zirconate thermal barrier coatings. *J Am Ceram Soc* 2020, **103**: 2048–2061.

[8] Vaßen R, Bakan E, Mack D, *et al.* Performance of YSZ and $Gd_2Zr_2O_7$/YSZ double layer thermal barrier coatings in burner rig tests. *J Eur Ceram Soc* 2020, **40**: 480–490.

[9] Lin YL, Zou LX, Dai JW, *et al.* First-principles application in the research field of thermal barrier coating, *Adv Ceram* 2025, **46**: 24–51.

[10] Zhang ZJ, Sun J, Liu GH, *et al.* High toughness and CMAS resistance of $REAlO_3/RE_2Zr_2O_7$ (RE = La, Nd, Sm, Eu, Gd, and Dy) composites with eutectic composition for thermal barrier coatings. *J Adv Ceram* 2024, **13**: 800–809.

[11] Cheng B, Zhang X, Zheng GB, *et al.* Improving the CMAS corrosion resistance of $Gd_2Zr_2O_7$ TBCs via laser simultaneously induced texture/featherlike/dense structures. *J Mater Res Technol* 2025, **36**: 10104–10117.

[12] Meng SJ, Guo L, Guo HB, *et al.* CMAS-phobic and infiltration-inhibiting protective layer material for thermal barrier coatings. *J Adv Ceram* 2024, **13**: 1254–1267.

[13] Yang WQ, Ye FX. The mechanical and thermal properties, CMAS corrosion resistance, and the wettability of novel thermal barrier material $GdTaO_4$. *Ceram Int* 2021, **47**: 28685–28697.

[14] Gan MD, Lu TL, Yu W, *et al.* Capturing and visualizing the phase transition mediated thermal stress of thermal barrier coating materials via a cross-scale integrated computational approach. *J Adv Ceram* 2024, **13**: 413–428.

[15] Cheng B, Yang GJ, Zhang Q, *et al.* Gradient thermal cyclic behaviour of $La_2Zr_2O_7$/YSZ DCL-TBCs with equivalent thermal insulation performance. *J Eur Ceram Soc* 2018, **38**: 1888–1896.

[16] Wang PF, Chen D, Wang QS, *et al.* Thermal stability and thermal cycling behavior of LGYYSZ/YSZ thermal barrier coatings fabricated by atmospheric plasma spraying. *Surf Coat Tech* 2025, **505**: 132038.

[17] Aziz HS, Huang MZ, Li ZY, *et al.* Repressing high-temperature radiative heat transfer in thermal barrier coatings. *J Am Ceram Soc* 2022, **105**: 3485–3497.

[18] Yang P, Yang DY, Hao EK, *et al.* Thermal shock resistance and failure analysis of $La_2(Zr_{0.75}Ce_{0.25})_2O_7$-based TBCs produced by atmospheric plasma spraying. *Surf Coat Tech* 2021, **409**: 126903.

[19] Mehboob G, Liu GL, Wang SJ, *et al.* Matching design of thickness ratio to extend the lifespan of double-layered thermal-barrier coatings. *Ceram Int* 2024, **50**: 1505–1518.

[20] Zhang H, Sun JB, Duo SW, *et al.* Thermal and mechanical properties of Ta_2O_5 doped $La_2Ce_2O_7$ thermal barrier coatings prepared by atmospheric plasma spraying. *J Eur Ceram Soc* 2019, **39**: 2379–2388.

[21] Zhang H, Yuan JY, Song WJ, *et al.* Composition, mechanical properties and thermal cycling performance of YSZ toughened $La_2Ce_2O_7$ composite thermal barrier coatings. *Ceram Int* 2020, **46**: 6641–6651.

[22] Zhao PS, Zheng HZ, Li GF, *et al.* Thermal cycling behavior of Yb^{3+}–Ce^{4+} Co-doped $La_2Zr_2O_7$-based TBCs: Experimental and theoretical research. *Corros Sci* 2024, **231**: 112003.

[23] Zhao YX, Li DC, Zhong XH, *et al.* Thermal shock behaviors of YSZ thick thermal barrier coatings fabricated by suspension and atmospheric plasma spraying. *Surf Coat Tech* 2014, **249**: 48–55.

[24] Chen DY, Dambra C, Dorfman M. Deposition, microstructure and thermal cycling performance of strain-tolerant thermal barrier coatings. *J Therm Spray Techn* 2023, **32**: 1108–1114.

[25] Wu MM, Liu Y, Qu WW, *et al.* Thickness-related failure behaviors of the thermal barrier coatings under thermal gradient cycling. *Surf Coat Tech* 2023, **468**: 129748.

[26] Guo J, Yin Y, Yi M. Extreme temperature gradient promoting oxygen diffusion in yttria-stabilized zirconia: A molecular dynamics study. *J Am Ceram Soc* 2024, **107**: 6783–6790.

[27] Dwivedi G, Viswanathan V, Sampath S, *et al.* Fracture toughness of plasma-sprayed thermal barrier ceramics: Influence of processing, microstructure, and thermal aging. *J Am Ceram Soc* 2014, **97**: 2736–2744.

[28] Zhu DM, Nesbitt JA, Barrett CA, *et al.* Furnace cyclic oxidation behavior of multicomponent low conductivity thermal barrier coatings. *J Therm Spray Techn* 2004, **13**: 84–92.

[29] Cao XQ, Vassen R, Stoever D. Ceramic materials for thermal barrier coatings. *J Eur Ceram Soc* 2004, **24**: 1–10.
[30] Vassen R, Cao XQ, Tietz F, *et al*. Zirconates as new materials for thermal barrier coatings. *J Am Ceram Soc* 2000, **83**: 2023–2028.
[31] Feng Y, Dong TS, Fu BG, *et al*. Thermal shock resistance of double-layer thermal barrier coatings. *J Mater Res* 2020, **35**: 2808–2816.
[32] Huang MZ, Liang J, Zhang P, *et al*. Opaque $Gd_2Zr_2O_7$/$GdMnO_3$ thermal barrier materials for thermal radiation shielding: The effect of polaron excitation. *J Mater Sci Technol* 2022, **100**: 67–74.
[33] Rai AK, Schmitt MP, Dorfman MR, *et al*. Comparison of single-phase and two-phase composite thermal barrier coatings with equal total rare-earth content. *J Therm Spray Techn* 2018, **27**: 556–565.
[34] Frommherz M, Scholz A, Oechsner M, *et al*. Gadolinium zirconate/YSZ thermal barrier coatings: Mixed-mode interfacial fracture toughness and sintering behavior. *Surf Coat Tech* 2016, **286**: 119–128.
[35] Si YC, Li LF, Wang RD, *et al*. Preparation, thermophysical properties and corrosion resistance of high-entropy rare earth tantalates ($5RE_{0.2}$)TaO_4 (RE=Y, Gd, Dy, Ce, Sm, La, Yb) ceramics as promising thermal barrier coating materials. *Ceram Int* 2025, **51**: 10783–10793.
[36] Bakan E, Mack DE, Mauer G, *et al*. Gadolinium zirconate/YSZ thermal barrier coatings: Plasma spraying, microstructure, and thermal cycling behavior. *J Am Ceram Soc* 2014, **97**: 4045–4051.
[37] Wei ZY, Cheng B, Wang J, *et al*. Extend the thermal cyclic lifetime of $La_2Zr_2O_7$/YSZ DCL TBCs by reducing modulus design on a toughening ceramic surface. *Surf Coat Tech* 2019, **374**: 134–143.
[38] Cheng B, Zhang YM, Yang N, *et al*. Sintering-induced delamination of thermal barrier coatings by gradient thermal cyclic test. *J Am Ceram Soc* 2017, **100**: 1820–1830.
[39] Wang Y, Guo HB, Gong SK. Thermal shock resistance and mechanical properties of $La_2Ce_2O_7$ thermal barrier coatings with segmented structure. *Ceram Int* 2009, **35**: 2639–2644.
[40] Dong HY, Wang DX, Pei YL, *et al*. Optimization and thermal cycling behavior of $La_2Ce_2O_7$ thermal barrier coatings. *Ceram Int* 2013, **39**: 1863–1870.
[41] Ma W, Dong HY, Guo HB, *et al*. Thermal cycling behavior of $La_2Ce_2O_7$/8YSZ double-ceramic-layer thermal barrier coatings prepared by atmospheric plasma spraying. *Surf Coat Tech* 2010, **204**: 3366–3370.
[42] Cheng B, Wang Y, Zhang X, *et al*. Sintering governing the cracking behaviors of different $La_2Zr_2O_7$/YSZ ceramic layer combination TBCs at 1150 °C. *Surf Coat Tech* 2021, **428**: 127910.
[43] Chen L, Wang S, Li C, *et al*. Durable RSZ/YSZ coatings with 1600 °C thermal shock resistance for rocket engine thrust chamber applications. *Ceram Int* 2025, **51**: 54903–54913.
[44] Mahade S, Curry N, Björklund S, *et al*. Durability of gadolinium zirconate/YSZ double-layered thermal barrier coatings under different thermal cyclic test conditions. *Materials* 2019, **12**: 2238.
[45] Mahade S, Curry N, Jonnalagadda KP, *et al*. Influence of YSZ layer thickness on the durability of gadolinium zirconate/YSZ double-layered thermal barrier coatings produced by suspension plasma spray. *Surf Coat Tech* 2019, **357**: 456–465.
[46] Feng XC, Guo FW, Luo LR, *et al*. Engineering design of feedstock powder and relevant thermal–mechanical performance of thermal/environmental barrier coatings. *J Adv Ceram* 2025, **14**: 9221033.
[47] Kelly MJ, Wolfe DE, Singh J, *et al*. Thermal barrier coatings design with increased reflectivity and lower thermal conductivity for high-temperature turbine applications. *Int J Appl Ceram Tec* 2006, **3**: 81–93.
[48] Hutchinson JW, Suo Z. Mixed mode cracking in layered materials. *Adv Appl Mech* 1991, **29**: 63–191.
[49] Jackson RW, Begley MR. Critical cooling rates to avoid transient-driven cracking in thermal barrier coating (TBC) systems. *Int J Solids Struct* 2014, **51**: 1364–1374.